Rise and fall of electron temperatures: Ohmic heating of ionospheric electrons from underdense HF radio wave pumping

B. Gustavsson,[1,2] M. T. Rietveld,[3] N. V. Ivchenko,[4] and M. J. Kosch[5]

Received 28 June 2010; revised 11 September 2010; accepted 15 September 2010; published 23 December 2010.

[1] Here we present electron temperature variations observed with incoherent scatter radar during a European Incoherent Scatter Scientific Association Heating experiment with high-frequency (HF) radio wave transmission at frequencies above the peak ionospheric critical frequency. The electron temperature increased from 2000 K up to 2800 K during the HF transmission periods. During the experiment both pump frequency and polarization were altered between pump pulses. The observed temperature variation is compared with numerical solutions to the electron energy equation with ohmic heating modeling the effect of the radio wave heating of the plasma. Agreement between observations and model is found to be good.

Citation: Gustavsson, B., M. T. Rietveld, N. V. Ivchenko, and M. J. Kosch (2010), Rise and fall of electron temperatures: Ohmic heating of ionospheric electrons from underdense HF radio wave pumping, *J. Geophys. Res.*, *115*, A12332, doi:10.1029/2010JA015873.

1. Introduction

[2] Cooling and heating of electrons control much of the energy flow in the ionosphere. To properly understand the energetics of the upper atmosphere and ionosphere it is necessary to be able to accurately model the heating and cooling processes of the electrons. In the ionosphere the dominating electron cooling processes are elastic collisions with ions, inelastic collisions with molecular nitrogen and oxygen exciting vibrational states, and excitation of the fine structure levels of atomic oxygen. The relative magnitude of the different channels for electron energy loss depends on electron temperature, T_e, and density and composition of the neutral atmosphere. Theoretically, electron cooling rates are calculated by collision integrals with measured collision cross sections multiplied with electron energy distributions, typically assumed to be Maxwellian. As the estimates of inelastic cross sections improve, cooling rates are updated; see *Pavlov* [1998a, 1998b], *Jones et al.* [2003], and *Campbell et al.* [2004] for the most recent advances in the continuous adjustments of electron cooling rates to molecular nitrogen and oxygen. Ohmic electron heating by high-frequency (HF) electromagnetic waves depends on wave amplitude and plasma conductivity, which in turn depend on the wave frequency and the effective electron collision frequency [*Sen and Wyller*, 1960; *Budden*, 1961]. Both cooling and heating depend on the shape of the electron distribution function. The common assumption that the electron distribution is Maxwellian in the ionosphere is not always good, since inelastic electron-neutral collisions modify the electron distribution, in particular the large cross section for excitation of vibrational states in N_2 between 2 and 3 eV cause significant reduction of the electron flux or a depletion of the electron distribution [*Carleton and Megill*, 1962; *Stubbe*, 1981]. This leads to large flux depletions in this energy range, mainly at low altitudes where the neutral density is high [*Stubbe*, 1981] but even at *F*-region altitudes the deviation can be approximately one order of magnitude at 2–4 eV [*Mishin et al.*, 2000; *Gustavsson et al.*, 2004; *Vlasov et al.*, 2004]. For high T_e, when the cooling is dominated by excitation of N_2 vibrations, such deviations from a Maxwellian electron distribution should lead to a significant modification of the electron cooling rates.

[3] When transmitting *X*-mode waves at frequencies above the critical frequency for reflection the only significant interaction between the pump wave and the ionospheric plasma is ohmic heating due to nonzero HF conductivity with an associated damping of the HF wave. No plasma resonances are excited, since there is no altitude where the pump frequency, f_0, is equal to the plasma frequency, f_p, or the upper hybrid frequency, f_{UH} ($f_{UH} = (f_p^2 + f_e^2)^{1/2}$, where f_e is the electron gyro frequency). Because there is no reflection of the pump wave there will be no reflected wave and thus no large-amplitude standing wave (for details on the standing waves at the ionospheric reflection altitude, see *Lundborg and Thidé* [1986]). There is only a slight beam swelling in the altitude range where the f_0 is close to f_p. Ohmic heating by HF radio waves with frequencies higher

[1]Department of Communications Systems, University of Lancaster, Lancaster, UK.
[2]Now at Space Environment Physics Group, School of Physics and Astronomy, University of Southampton, Southampton, UK.
[3]EISCAT Scientific Association, Ramfjordmoen, Norway.
[4]Space and Plasma Physics, School of Electrical Engineering, Royal Institute of Technology, Stockholm, Sweden.
[5]Department of Physics, InfoLab21 University of Lancaster, Lancaster, UK.

0148-0227/10/2010JA015873

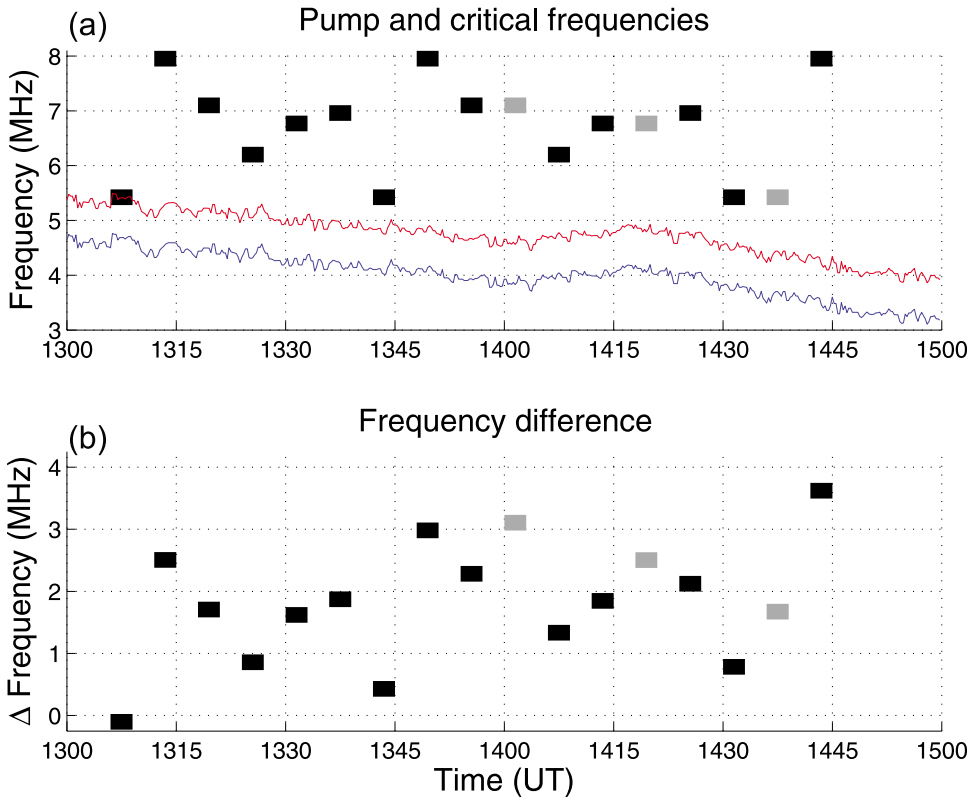

Figure 1. (a) The frequencies of the HF-on periods are shown with black (*X* mode) and gray (*O* mode) bars together with the slowly decreasing ionospheric critical frequencies in red (*X* mode) and blue (*O* mode). (b) The frequency offset above the critical frequencies is displayed, showing that for all pulses except the first the HF transmission frequency was well above the critical frequency.

than the peak plasma frequency has previously been studied for relatively low effective radiated power (ERP) in a very low density *F*-region ionosphere [*Löfås et al.*, 2009], where T_e enhancements of 300–400 K were observed. For overdense conditions the effects of ohmic heating have been studied both theoretically and experimentally [*Shoucri et al.*, 1984; *Hansen et al.*, 1992a, 1992b]. However, due to the large electric fields and the matching of f_0 to f_p at the reflection altitude, or f_{UH}, a few kilometers below, a great number of plasma resonances dissipate energy from the pump wave [see *Gurevich*, 2007, and references therein]. In such conditions much of the *F*-region energy deposition and electron heating occurs just below the reflection altitude [*Robinson*, 1989] and is due to nonohmic processes. From there heat is convected up and down along the magnetic field [*Mantas et al.*, 1981; *González et al.*, 2005]. The exact amount of energy deposited in the ionospheric electrons in this region is therefore difficult to calculate accurately from first principles.

[4] Transmission of HF radio waves with frequencies above the ionospheric critical frequency contributes with a heat source that is possible to estimate quantitatively from theory. Thus the physical models of both electron cooling and heating can be investigated. Here we present T_e observation from an experiment with ERP between 450 and 870 MW with f_0 well above the *F*-region critical frequency. These observations are compared with the theoretical response to ohmic heating of ionospheric plasma. The comparison show that the modeled T_e agrees well with the observations. This indicates that the electron cooling rates as well as the plasma conductivity are good enough for T_e between 1000 and 3000 K.

2. Experiment and Observations

[5] To study the ionospheric response to ohmic heating and its variation with pump frequency we performed an

Table 1. HF Transmission Sequence

HF Pulse (UT)	*f* (MHz)	ERP (MW)	Polarization
1306	5.423	221	X
1312	7.953	389	X
1318	7.1	325	X
1324	6.2	232	X
1330	6.77	304	X
1336	6.96	315	X
1342	5.423	223	X
1348	7.953	407	X
1354	7.1	324	X
1400	7.1	314	O
1406	6.2	234	X
1412	6.77	302	X
1418	6.77	282	O
1424	6.96	315	X
1430	5.423	224	X
1436	5.423	215	O
1442	7.953	410	X

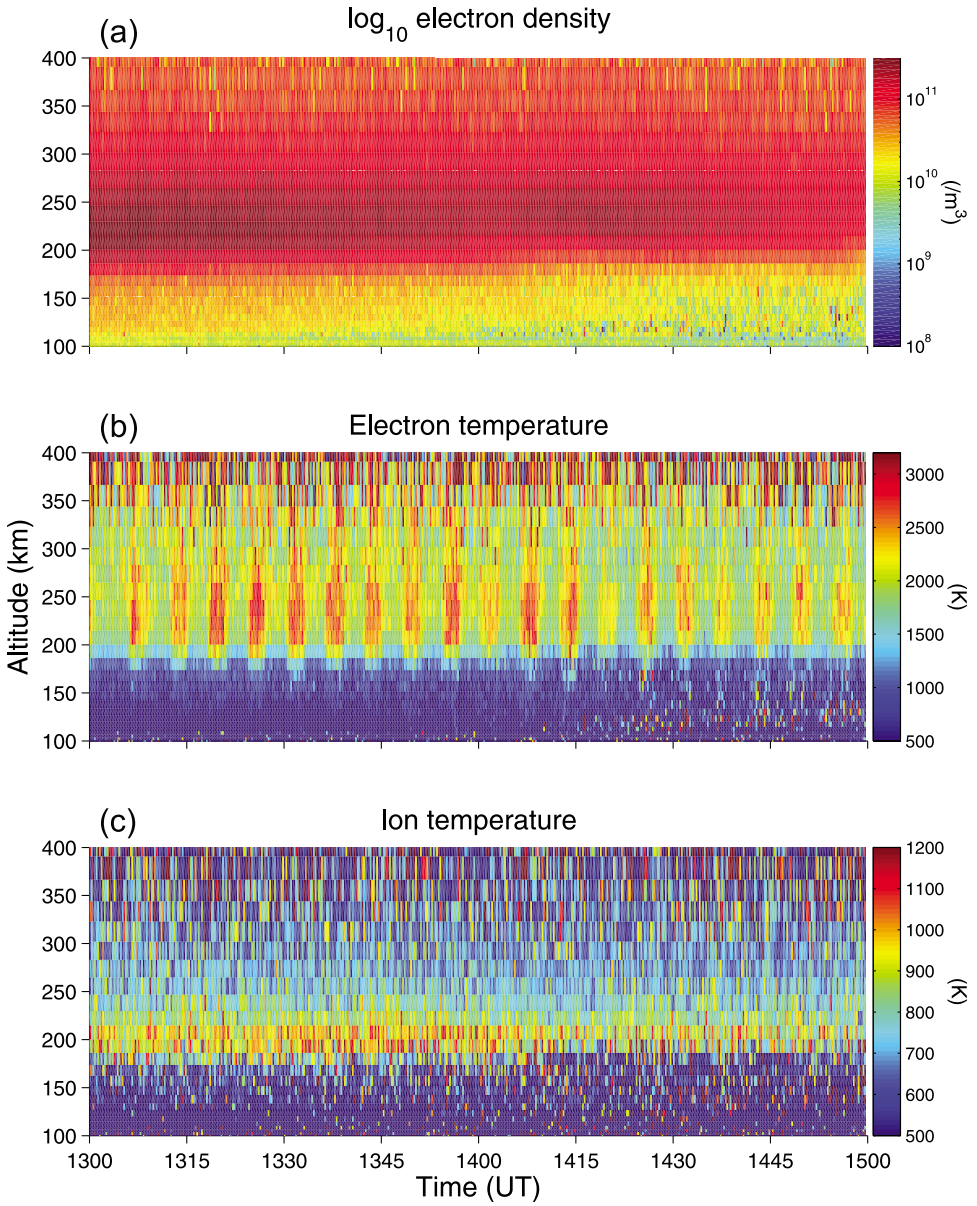

Figure 2. From 13:00:00 to 15:00:00 UT on 27 October 2008 the EISCAT UHF IS radar observed the (a) electron density (n_e), (b) electron, and (c) ion temperatures (T_e and T_i, respectively) during a Heating experiment with a HF pump cycle of 3 min on and 3 min off.

experiment on 27 October 2008 at the European Incoherent Scatter Scientific Association (EISCAT) heating facility [*Rietveld et al.*, 1993]. From 13:06 to 15:00 UT EISCAT Heating, located in northern Norway (69.6°N, 19.2°E), was operated in a 180 s on/180 s off cycle transmitting between 450 and 870 MW ERP in the magnetic zenith at six frequencies between 5.35 and 7.95 MHz, as shown in Figure 1 and Table 1.

[6] The ionospheric response to the HF transmission was observed with the EISCAT ultra-high-frequency (UHF) radar running the Beata (version 1.2) radar pulse code giving time and altitude resolution of 5 s and 15–20 km in the *F* region, here postintegrated to 15 s time resolution to reduce measurement noise. Over the course of the experiment the *F*-region electron density, n_e, decreased slowly, as can be seen in Figure 2, leading to a steady decrease in *X*- and *O*-mode critical frequencies from $f_X F2 = 5.4$ MHz ($f_O F2 = 5.0$ MHz) at 1300 UT to 4 MHz (3.4 MHz) at 1500 UT. At altitudes below 150 km the electron density, n_e, remained low throughout the experiment, leading to low *D*-region absorption of the HF wave. As can be seen in Figure 1, the pump frequency was well above the *X*-mode critical frequency, $f_X F2$, with δf ($\delta f = f_0 - f_X$ F2, and $\delta f = f_0 - f_O$ F2 respectively) between 0.35 and 3.8 MHz from the second HF-on period. For all HF-on periods the transmission was in *X* mode, except the pump periods starting at 1400, 1418, and 1436 UT, where the transmission was in *O* mode.

[7] During the HF-on periods T_e increased to more than 2800 K from background temperatures around 2000 K at the *F*-region peak, as can be seen in Figure 2. The temperature

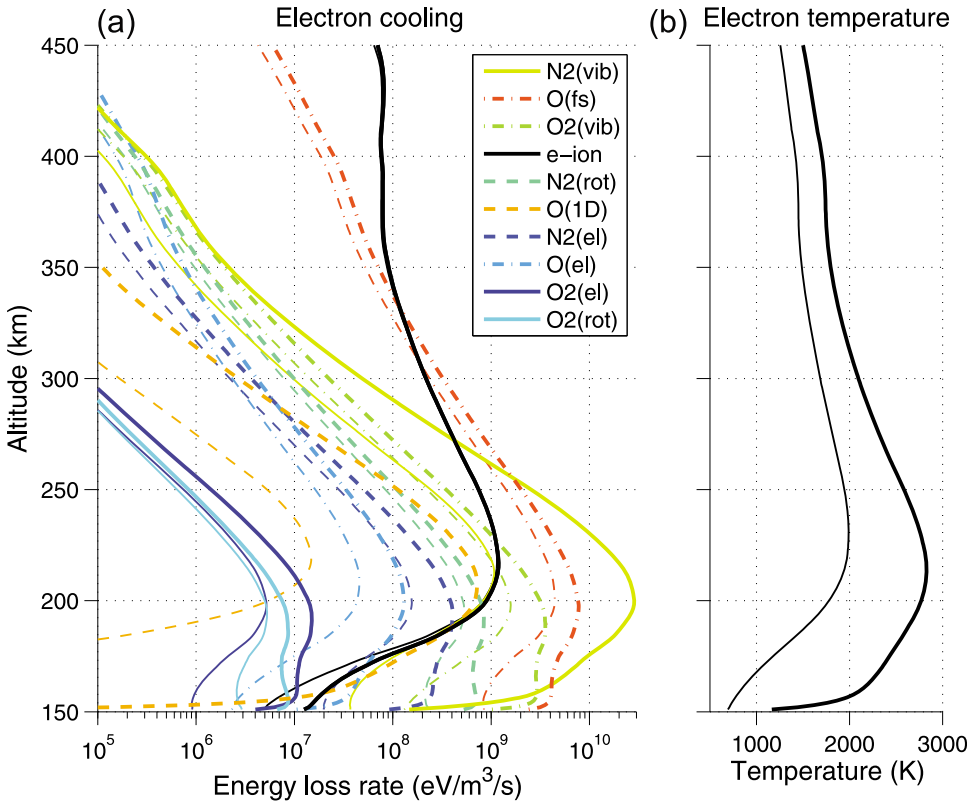

Figure 3. The altitude variation of electron energy loss rates shown for (a) HF-heated T_e with bold curves and (b) background T_e with thin curves. The corresponding T_e profiles are shown in the right panel.

enhancements are clearly visible from 170 to 320 km altitude. Neither ion temperature, T_i, nor field aligned ion drift, v_i, were modified by the radio transmission.

3. Modeling

[8] For the "overdense" case where the pump wave is reflected, the ionospheric response to HF heating on thermal timescales has to be modeled with the coupled ion and electron continuity, momentum, and energy equations [e.g., *Shoucri et al.*, 1984; *Hansen et al.*, 1992b, 1992a]. For the underdense conditions of our experiment, the HF heating is smoothly distributed in altitude and there are no sharp gradients in plasma pressure, so there will be no significant density modulations. Our observations also show no detectable change in T_i during the HF transmission, and the ionospheric response can be well modeled with a one-dimensional electron energy equation [*Löfås et al.*, 2009].

3.1. Ohmic Electron Heating

[9] For under dense conditions the ionospheric response to HF radio wave transmissions can be modeled with just a one-dimensional electron energy equation. After *Shoucri et al.* [1984] we have

$$\frac{3}{2}k_B n_e\left(\frac{\partial T_e}{\partial t}+(v_e\bar{z})\frac{\partial T_e}{\partial z}\right)+k_B n_e T_e\frac{\partial}{\partial z}(v_e\bar{z}) = \frac{\partial}{\partial z}\left[\kappa_e\frac{\partial T_e}{\partial z}\right]+Q_{\mathrm{HF}}(T_e,z,t)+Q_0(z,t)-L(T_e,z,t), \quad (1)$$

where $\bar{z}$ is aligned with the local magnetic field, κ_e is the electron heat conductivity, Q_{HF} is the HF pump wave energy deposition to the electrons, Q_0 is the background electron heating (mainly from photoelectrons), and L is the electron cooling rate. The dominant cooling processes in the HF-heated ionosphere are excitation of vibrational states in N_2 [*Pavlov*, 1998a], excitation of fine structure levels in atomic oxygen [*Dalgarno*, 1968; *Carlson and Mantas*, 1982], excitation of vibrational states in O_2 [*Pavlov*, 1998b], and elastic electron-ion collisions [e.g., *Rees and Roble* 1975], as shown in Figure 3. If we take into account the very low field aligned plasma drift measured by EISCAT the convective terms are found to be insignificantly small and equation (1) can be further simplified [*Löfås et al.*, 2009] to

$$\frac{3}{2}k_B n_e\frac{\partial T_e}{\partial t}=\frac{\partial}{\partial z}\kappa_e(T_e,z,t)\frac{\partial T_e}{\partial z} + Q_{\mathrm{HF}}(T_e,z,t)+Q_0(z,t)-L(T_e,z,t). \quad (2)$$

For underdense conditions Q_{HF} will consist of ohmic heating only, since there can be no pump-wave-driven instabilities because f_0 will be well above both f_p and f_{UH} at all altitudes. Ohmic heating is the time average of the product between the pump-wave electrical field and the induced current, which can be calculated as:

$$Q_{\mathrm{HF}}=\frac{1}{2}\mathbf{Re}[\mathbf{E}^*\cdot\bar{\sigma}\cdot\mathbf{E}]. \quad (3)$$

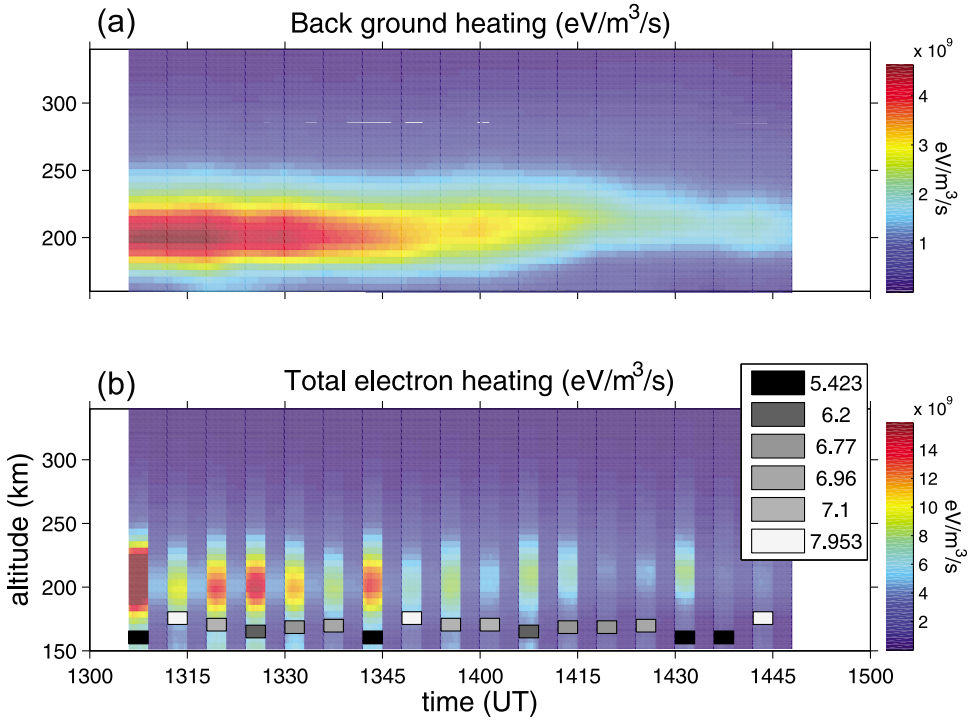

Figure 4. (a) The estimate of the background electron heating, showing the slow decrease and rise of the lower border of electron heating both consistent with increasing solar zenith angle and reduced photoelectron production. (b) The estimated total electron heating where the ohmic heating, Q_{HF}, of the HF pump wave is decreasing during the experiment due to the decreasing F-region electron critical frequency. Q_{HF} is larger for HF transmission periods with lower frequencies (marked with darker gray bars at lower altitudes in this and subsequent figures), even though the ERP increases with f_0.

Here $\bar{\sigma}$ is the conductivity tensor and the wave electrical field **E** at altitude z is

$$E_{\pm} = E(z_0)\left(\frac{z_0}{z}\right)\left[\frac{\epsilon_{\pm}(z_0)}{\epsilon_{\pm}(z)}\right]^{1/4} \exp\left\{ik_0 \int_{z_0}^{z} \mathcal{N}_{\pm}(z)dz\right\}, \quad (4)$$

where $\epsilon_{\pm}$ is the dielectric tensor, $\mathcal{N}_{\pm}$ is the refractive index, and k_0 is the vacuum wave number of the pump wave. In our modeling we calculate the wave electrical field at the bottom of the ionosphere (z_0 = 150 km) taking 2 dB D-region absorption into account.

3.2. Background Electron Heating

[10] When integrating the electron energy equation (2) we need an estimate of the background electron heating, Q_0, in addition to estimates of the transmitted ERP and electron cooling rates. By rewriting equation (2) for HF off conditions, we get

$$Q_0 = \frac{3}{2}k_B n_e \frac{\partial T_e}{\partial t} - \frac{\partial}{\partial z}\kappa_e \frac{\partial T_e}{\partial z} + L. \quad (5)$$

Here we can use the EISCAT observations of n_e and T_e at the end of each HF off period to get an estimate of Q_0. The noise in the observations leads to errors in Q_0, in particular through the $\frac{\partial}{\partial z}\kappa_e \frac{\partial T_e}{\partial z}$ term. Direct use of Q_0 derived from observations leads to errors in the steady state T_e. By adjusting Q_0 for each HF off period with a correction factor ($0.85 < C < 1.5$) we get a Q_0, shown in the upper panel of Figure 4, for which integration of equation (2) gives a good fit of T_e for steady-state conditions at the end of the HF off periods. The estimates of Q_0 are essentially obtained by equating Q_0 with the electron cooling rates and thus obviously depend on the neutral atmospheric densities. In Appendix A we show that the neutral densities can be estimated from the observations by comparing Q_0 with electron heating from photoelectrons.

3.3. Results: Observations Fit the Modeling

[11] Integration of the electron energy equation (2) with T_e at 150 km and $\partial T_e/\partial z$ at 450 km as boundary conditions and T_e at 13:05:45–13:06:00 UT as initial condition gives T_e, shown in Figure 5, that varies with time and altitude in good agreement with the EISCAT UHF T_e observations.

[12] The T_e obtained by integrating the electron energy equation with ohmic heating by the HF pump wave, shown in the middle panel of Figure 5, agree well with the observed T_e, both the rise and fall characteristics and the variation of the T_e enhancements between different HF pulses, where the pump frequency, ERP and polarization varied. The standard deviation of the residual between the observed and modeled T_e calculated for the altitude range 150 to 300 km is approximately 180 K (≈9%), which is comparable to the measurement noise of T_e; while the average residual is −70°K (≈4%) and the only systematic discrepancies occur for the pump pulses with X-mode transmission at the lowest frequency, 5.423 MHz. In the bottom panel it is clearly seen that the only pulse where there is a significant discrepancy

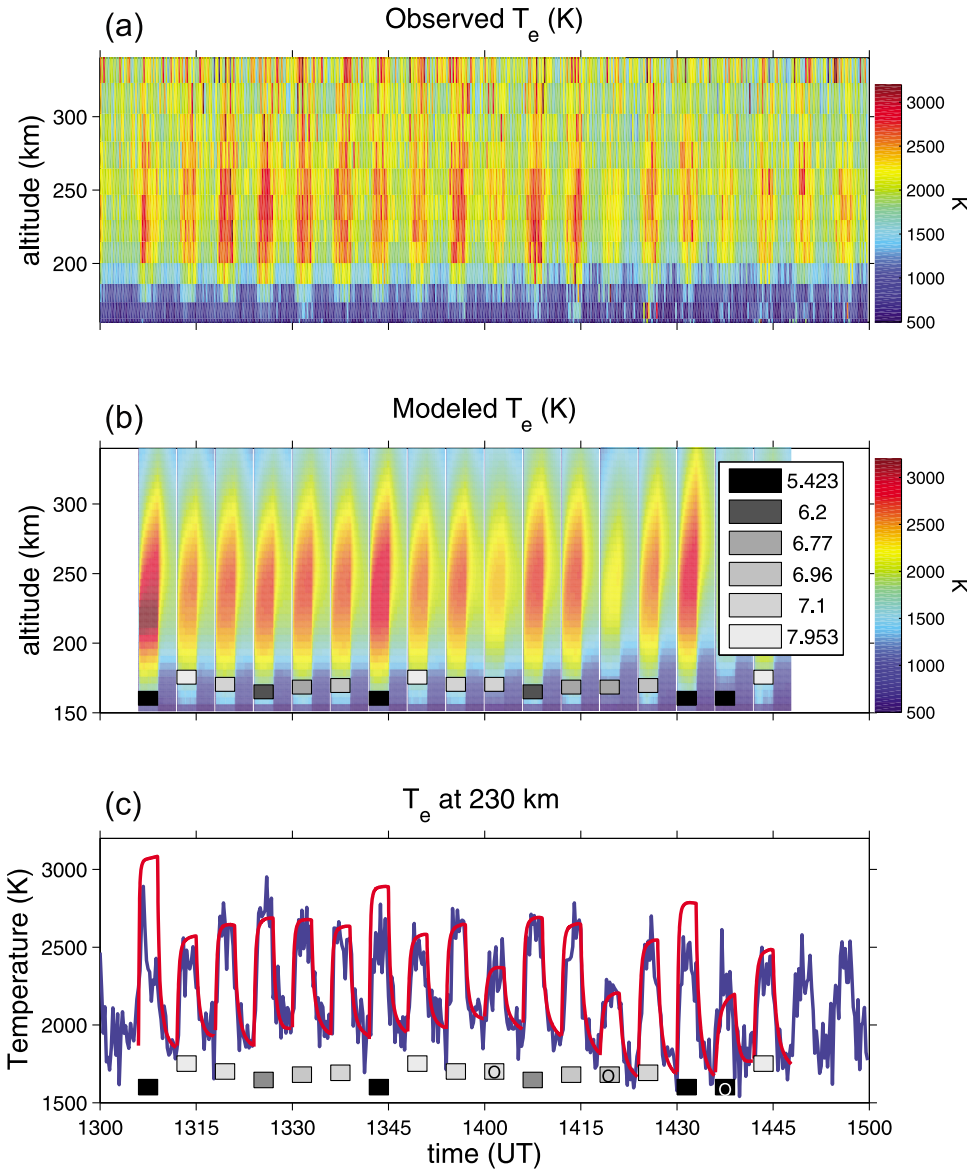

Figure 5. (a) The observed T_e variations agree well with the solution to the electron energy equation with ohmic heating by the HF pump wave; (b) both the temporal characteristics and the variation between different HF pulses, where the pump frequency, power, and polarization varied. (c) It is clearly seen that the only pulse where there is a significant discrepancy between observations (blue curve) and modeling (red curve) results is the first pump period. For this transmission period it is likely that the transmitted frequency was just at or below the *X*-mode critical frequency, leading to reflection of the pump wave.

between observations and modeling results is the first pump period. For this transmission period it is likely that the transmitted frequency was just at or below the *X*-mode critical frequency, leading to reflection of the pump wave.

4. Summary, Conclusion, and Outlook

[13] Underdense EISCAT Heating produced T_e increases of up to 800 K, with transmission of 450 to 870 MW ERP at frequencies well above the ionospheric critical frequencies.

[14] As can be seen in Figure 4 the variation in ERP and conductivity leads to a variation in ohmic heating that reproduces the observed T_e accurately when used in a one-dimensional electron energy equation with HF transmission in a 5.423–7.95 MHz frequency range with polarization in both *X* mode and *O* mode.

[15] The good agreement of the model indicates that the electron collision frequencies [e.g., *Schunk and Nagy* 1978] and electron cooling rates [*Pavlov*, 1998a, 1998b; *Pavlov and Berrington*, 1999] are sufficiently good for T_e from 1000 to 3000 K. Further, because the modeled T_e agrees well with the observations for electron densities varying by a factor of 2, the relative contribution between electron energy losses to ions (proportional to n_e^2) and neutrals (proportional to n_e) is accurately estimated. Likewise, the variation of ohmic heating with polarization, f_0, and the difference between f_0 and f_p is accurately estimated.

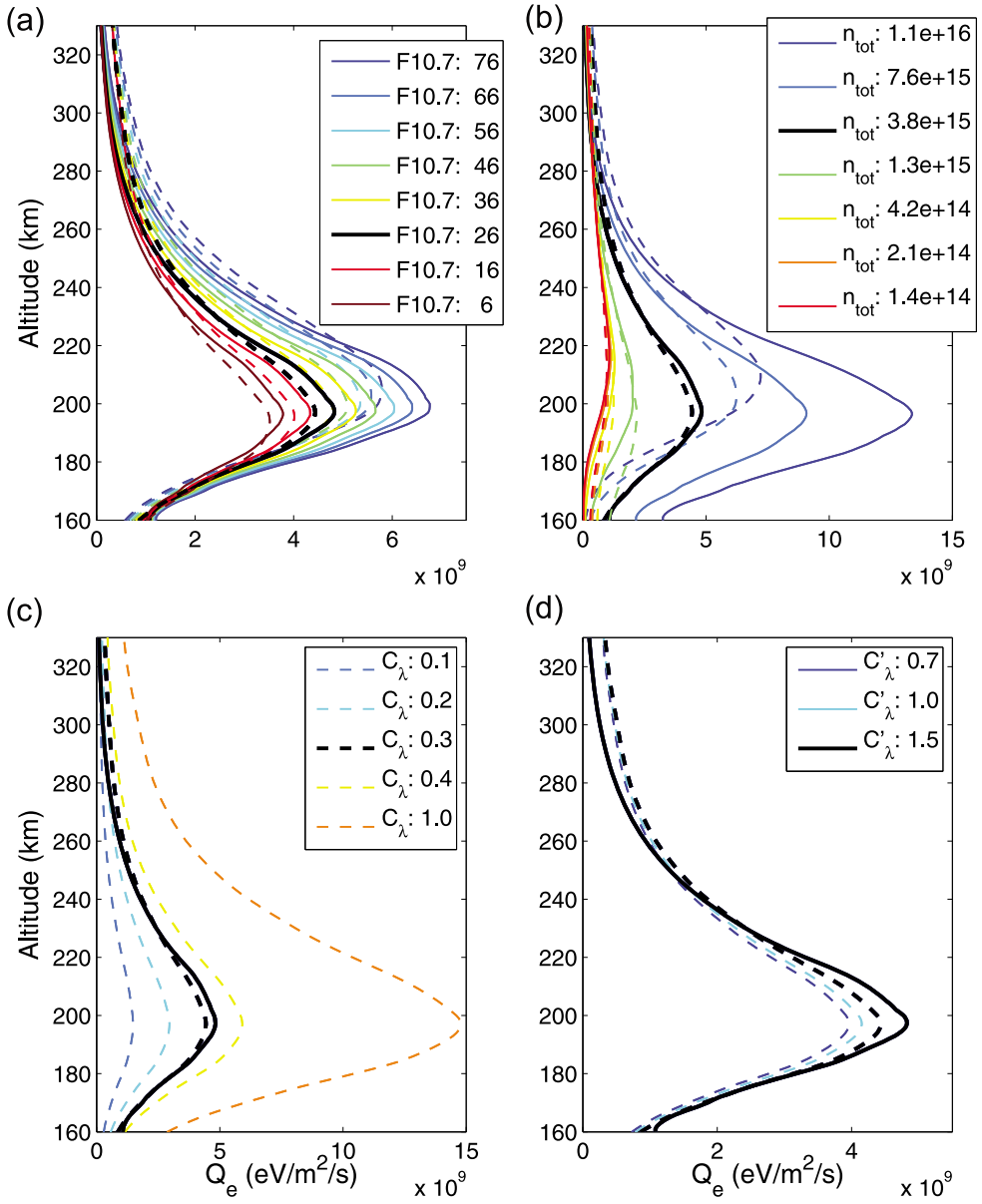

Figure 6. (a) The altitude variation of Q_0, solid, and Q_{e*}, dashed, for varying neutral temperature at 200 km, with the best fit shown in black. Here the best fit for neutral density and solar EUV scaling factors have been used. (b) The variation of Q_0 and Q_{e*} with neutral density at 200 km is shown. The variation of Q_0, solid, and Q_{e*} with scaling factors for SOLAR2000 EUV fluxes (c) below 1200 Å and (d) below 250 Å is shown, respectively.

[16] The large T_e modulations show that ohmic heating at frequencies above $f_X F2$ can be used to heat the ionospheric plasma without driving instabilities, exciting turbulence, or creating striations. This makes it possible to use underdense heating to preheat the ionospheric electrons and then switch to "normal" overdense *O*-mode transmission and investigate the T_e variation for onset characteristics of stimulated (or secondary) electromagnetic emissions (SEE), radio-induced optical emissions, and striations/coherent backscatter.

[17] Finally, we suggest that it should be possible to use ISR observations of T_e to estimate background electron heating by using the electron energy equation (equation 5) and photoelectron modeling, at least during quiet conditions. This would make it possible to monitor variation of the thermospheric densities and the energy input into the ionosphere, mainly from solar EUV.

Appendix A: Electron Heating as a Means to Estimate Neutral Densities and Solar EUV Fluxes

[18] Q_0 estimated from equation (5) is essentially obtained by equating Q_0 with the electron cooling rate (with corrections for the gradients in T_e), which depends on the neutral atmosphere density. For day-time *F*-region conditions the electron heating is dominated by photoelectron electron heating, Q_{e*} [*Schunk and Nagy*, 1978]. Since the photoionization rate depends on the neutral density and the EUV photon flux, the amplitude and altitude variation of Q_{e*} also

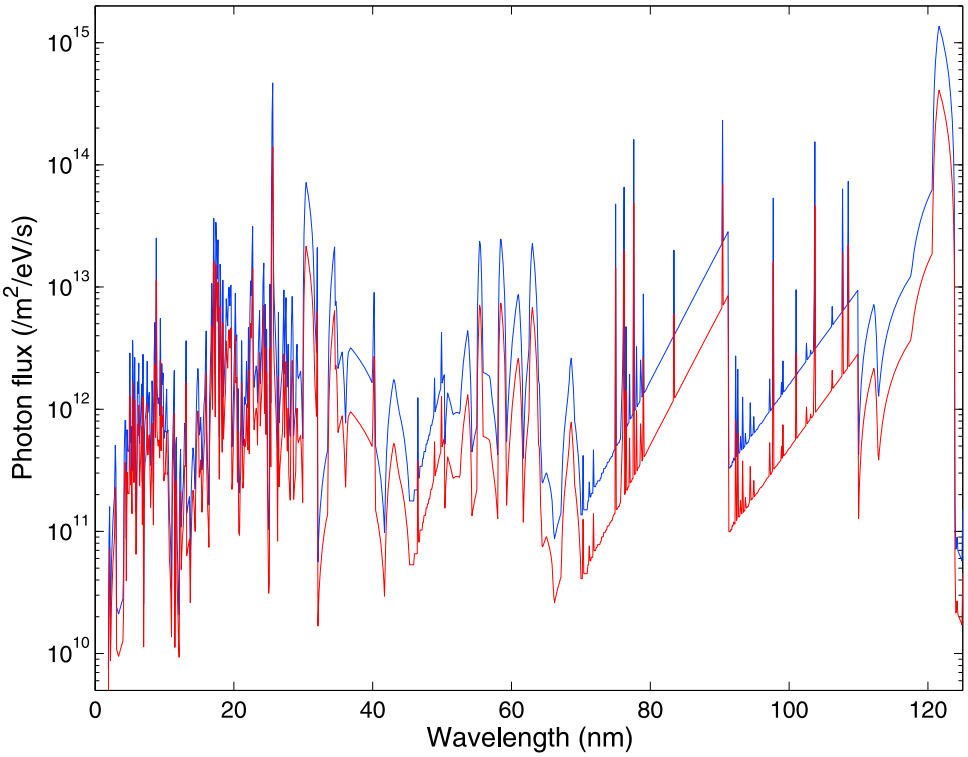

Figure 7. The SOLAR2000 EUV spectra for 20081027 is presented in blue, and the spectra scaled with a factor 0.3 above 250 Å and a factor 0.45 below 250 Å is presented in red.

depends on the neutral atmosphere density. Searching for an atmospheric density profile and a solar EUV spectra that gives the best fit between Q_0 and Q_{e*} gives estimates of both the heat sources and the neutral atmosphere. As shown in Figure 6, both the amplitude and the altitude of the peak heating rates varies differently for Q_0 and Q_{e*} with thermospheric temperature density and solar EUV photon flux.

[19] The photoelectron electron heating is

$$Q_{e*} = n_e(z) \int_{E_c}^{\infty} L_{ee}(E,z) I_e(E,z) dE, \qquad \text{(A1)}$$

where $I_e(E, z)$ is the photoelectron flux at altitude z and energy E and L_{ee} is the electron stopping cross section or loss function [*Swartz et al.*, 1971]

$$L_{ee}(E) = \frac{3.37 \times 10^{-12}}{E^{0.94} n_e^{0.03}} \left(\frac{E - T*}{E - 0.53T*} \right)^{2.36} \text{eV cm}^2, \qquad \text{(A2)}$$

where $T*$ is the electron temperature in eV. The photoelectron flux is calculated with with an electron-two-stream code [*Gustavsson and Eliasson*, 2008]. The photoelectron production we calculate with photoionization cross sections compiled by *Itikawa et al.* [1986, 1989] and *Itikawa and Ichimura* [1990] and solar EUV fluxes from SOLAR2000 [*Tobiska and Bouwer*, 2006] with one scale factor for wavelengths below 1200 Å and another for wavelengths below 250 Å. In Figure 7 the scaled EUV photon fluxes are shown together with the EUV fluxes from SOLAR2000. For the altitude variation of the neutral atmosphere we use the MSIS-90 [*Hedin*, 1991] with a range of F10.7 fluxes, to get a span of thermospheric temperatures and an additional scaling factor for the thermospheric densities.

[20] Fitting Q_0 and Q_{e*} by adjusting the neutral densities and solar EUV photon fluxes makes it possible to obtain estimates of the day-to-day variations of both the thermospheric densities and the solar EUV flux. The models currently in use for both are good in a statistical sense but known to have considerable uncertainty for any particular day [*Peterson et al.*, 2009; *Hedin*, 1991], so even if there are systematic errors in the photo-ionization or electron collision cross sections this method should make it possible to at least obtain relative day-to-day correction factors to both MSIS-90 and solar2000.

[21] **Acknowledgments.** EISCAT is funded by the research councils of China (CRIRP), Finland (SA), Germany (DFG), Japan (NIPR and STEL), Norway (NFR), Sweden (VR), and the United Kingdom (NERC). The authors thank the referees for their encouraging and helpful comments.

[22] Robert Lysak thanks Todd Pedersen and another reviewer for their assistance in evaluating this manuscript.

References

Budden, K. G. (1961), *Radio Waves in the Ionosphere*, Cambridge University Press, London, U. K.

Campbell, L., M. J. Brunger, D. C. Cartwright, and P. J. O. Teubner (2004), Production of vibrationally excited N_2 by electron impact, *Planet. Space Sci.*, *52*, 815–822, doi:10.1016/j.pss.2004.03.004.

Carleton, N. P., and L. R. Megill (1962), Electron energy distribution in slightly ionized air under the influence of electric and magnetic fields, *Phys. Rev.*, *126*(6), 2089–2099, doi:10.1103/PhysRev.126.2089.

Carlson, H. C., Jr., and G. P. Mantas (1982), An experimental test of the ionosphere electron gas cooling rate by excitation of the fine structure of the ground state of atomic oxygen, *J. Geophys. Res.*, *87*, 4515–4524.

Dalgarno, A. (1968), Inelastic collisions at low energies, *Can. J. Chem.*, *47*, 1723–1731.

González, S. A., M. J. Nicolls, M. P. Sulzer, and N. Aponte (2005), An energy balance study of the lower topside ionosphere using the Arecibo incoherent scatter radar and heating facilities, *J. Geophys. Res.*, *110*, A11303, doi:10.1029/2005JA011154.

Gurevich, A. V. (2007), Reviews of topical problems: Nonlinear effects in the ionosphere, *Soviet Physics Uspekhi*, *50*, 1091–1121, doi:10.1070/PU2007v050n11ABEH006212.

Gustavsson, B., and B. Eliasson (2008), Hf radio wave acceleration of ionospheric electrons: Analysis of hf-induced optical enhancements, *J. Geophys. Res.*, *113*, A08319, doi:10.1029/2007JA012913.

Gustavsson, B., T. Sergienko, I. Häggström, and F. Honary (2004), Simulation of high energy tail of electron distribution function, *Adv. Polar Upper Atmos. Res.*, *18*(18), 1–9.

Hansen, J. D., G. J. Morales, L. M. Duncan, and G. Dimonte (1992a), Large-scale HF-induced ionospheric modifications: Experiments, *J. Geophys. Res.*, *97*, 113–122.

Hansen, J. D., G. J. Morales, and J. E. Maggs (1992b), Large-scale HF-induced ionospheric modifications: Theory and modeling, *J. Geophys. Res.*, *97*, 17,019–17,032.

Hedin, A. (1991), Extension of the MSIS thermospheric model into the middle and lower atmosphere, *J. Geophys. Res.*, *96*(A2), 1159–1172.

Itikawa, Y., and A. Ichimura (1990), Cross sections for collisions of electrons and photons with atomic oxygen, *J. Phys. Chem. Ref. Data*, *19*(3), 637–651.

Itikawa, Y., M. Hayashi, A. Ichimura, K. Onda, K. Sakimoto, K. Takayanagi, M. Nakamura, H. Nishimura, and T. Takayanagi (1986), Cross sections for collisions of electrons and photons with nitrogen molecules, *J. Phys. Chem. Ref. Data*, *15*(3), 985–1010.

Itikawa, Y., A. Ichimura, K. Onda, K. Sakimoto, K. Takayanagi, Y. Hatano, M. Hayashi, H. Nishimura, and S. Tsurubuchi (1989), Cross sections for collisions of electrons and photons with oxygen molecules, *J. Phys.Chem. Ref. Data*, *18*, 23–42.

Jones, D. B., L. Campbell, M. J. Bottema, and M. J. Brunger (2003), New electron-energy transfer rates for vibrational excitation of O_2, *New J. Phys.*, *5*, 114.1–114.11, doi:10.1088/1367-2630/5/1/114.

Löfås, H., N. Ivchenko, B. Gustavsson, T. B. Leyser, and M. T. Rietveld (2009), F-region electron heating by X-mode radiowaves in underdense conditions, *Ann. Geophys.*, *27*(6), 2585–2592.

Lundborg, B., and B. Thidé (1986), Standing wave pattern of HF radio waves in the ionospheric reflection region. II - Applications, *Radio Sci*, *21*, 486–500.

Mantas, G. P., H. C. Carlson, and C. H. LaHoz (1981), Thermal response of the F region ionosphere in artificial modification experiments by HF radio waves, *J. Geophys. Res.*, *86*(A2), 561–574.

Mishin, E., H. C. Carlson, and T. Hagfors (2000), On the electron distribution function in the F region and airglow enhancements during HF modification experiments, *Geophys. Res. Lett.*, *27*(18), 2857–2860.

Pavlov, A. V. (1998a), New electron energy transfer rates for vibrational excitation of N_2, *Ann. Geophys.*, *16*, 176–182.

Pavlov, A. V. (1998b), New electron energy transfer and cooling rates by excitation of O_2, *Ann. Geophys.*, *16*, 1007–1013.

Pavlov, A. V., and K. A. Berrington (1999), Cooling rate of thermal electrons by electron impact excitation of fine structure levels of atomic oxygen, *Ann. Geophys.*, *17*, 919–924.

Peterson, W. K., E. N. Stavros, P. G. Richards, P. C. Chamberlin, T. N. Woods, S. M. Bailey, and S. C. Solomon (2009), Photoelectrons as a tool to evaluate spectral variations in solar euv irradiance over solar cycle timescales, *J. Geophys. Res.*, *114*, A10304, doi:10.1029/2009JA014362.

Rees, M. H., and R. G. Roble (1975), Observations and theory of the formation of stable auroral red arcs., *Rev. Geophys. Space Phys.*, *13*, 201–242.

Rietveld, M. T., H. Kohl, H. Kopka, and P. Stubbe (1993), Introduction to ionospheric heating at Tromsø —I. experimental overview, *J. Atmos. Terr. Phys.*, *55*(4), 577–599.

Robinson, T. R. (1989), The heating of the high latitude ionosphere by high power radio waves, *Phys. Rep.*, *179*, 79–209.

Schunk, R. W., and A. F. Nagy (1978), Electron temperatures in the *f* region of the ionosphere: Theory and observations, *Rev. Geophys.*, *16*(16), 355–399, doi:10.1029/RG016i003p00355.

Sen, H. K., and A. A. Wyller (1960), On the Generalization of the Appleton-Hartree Magnetoionic Formulas, *J. Geophys. Res.*, *65*, 3931–3950, doi:10.1029/JZ065i012p03931.

Shoucri, M. M., G. J. Morales, and J. E. Maggs (1984), Ohmic heating of the polar F region by HF pulses, *J. Geophys. Res.*, *89*, 2907–2917.

Stubbe, P. (1981), Modifying effects of a strong electromagnetic wave upon a weakly ionized plasma: A kinetic description, *Radio Sci.*, *16*(3), 417–425.

Swartz, W. E., J. S. Nisbet, and A. E. S. Green (1971), Analytic expression for the energy-transfer rate from photoelectrons to thermal electrons., *J. Geophys. Res.*, *76*(34), 8475–8480.

Tobiska, W. K., and S. D. Bouwer (2006), New developments in SOLAR2000 for space research and operations, *Adv. Space Res.*, *37*, 347–358, doi:10.1016/j.asr.2005.08.015.

Vlasov, M. N., M. C. Kelley, and E. Gerken (2004), Impact of vibrational excitation on ionospheric parameters and artificial airglow during HF heating in the F region, *J. Geophys. Res.*, *109*, A09304, doi:10.1029/2003JA010316.

B. Gustavsson, Space Environment Physics Group, School of Physics and Astronomy, University of Southampton, Highfield, Southampton SO17 1BJ, UK. (bjorn@irf.se)

N. V. Ivchenko, Space and Plasma Physics, School of Electrical Engineering, Royal Institute of Technology, Teknikringen 31, Stockholm SE-10044, Sweden.

M. J. Kosch, Department of Physics, InfoLab21, University of Lancaster, South Drive, Lancaster LA1 4WA, UK.

M. T. Rietveld, EISCAT Scientific Association, N-9027 Ramfjordbotn, Norway.